

Enhanced slow light propagation in photonic crystal waveguides using angular properties of scatter elements

Daobin Wang (王道斌)^{1,2*}, Jie Zhang (张杰)², Yongli Zhao (赵永利)², Sai Chen (陈赛)², Lihua Yuan (元丽华)¹, Jingli Lei (雷景丽)¹, Cairong Zhang (张材荣)¹, and Shanglin Hou (侯尚林)¹

¹School of Science, Lanzhou University of Technology, Lanzhou 730050, China

²State Key Laboratory of Information Photonics and Optical Communications, Beijing University of Posts and Telecommunications, Beijing 100876, China

*Corresponding author: cougarlz@gmail.com

Received May 23, 2012; accepted July 13, 2012; posted online November 30, 2012

Applicability of the angular properties of scatter elements as a tool to achieve improved slow light performance with small group velocity dispersion and large bandwidth in photonic crystal waveguides is investigated. A polyatomic photonic crystal waveguide, including two scatter elements with different geometrical shapes in each primitive cell, is proposed to investigate the feasibility of our method. Numerical results show that a versatile control of the dispersion relation of slow light modes, with large normalized delay-bandwidth products ranging from 0.2085 to 0.3394, can be obtained using a unique geometrical parameter.

OCIS codes: 230.5298, 250.5530, 160.5293.

doi: 10.3788/COL201210.122301.

Slow light has attracted considerable interest over the past decade, primarily because of the ground breaking successes of achieving slow propagation velocity^[1] and stopping light entirely^[2]. Based from these pioneering results, a substantial amount of work, which attained the slow light propagation in diverse media, such as metal vapors with and without electromagnetically induced transparency, rare-earth-doped materials, Raman and Brillouin fiber optical amplifiers, photonic crystal waveguides, and micro-resonators, have been performed in recent years. In particular, slow light in photonic crystals has recently become a hot topic because of its numerous merits, such as room-temperature operability and easy on-chip integration.

However, slow light in a photonic crystal waveguide is usually accompanied by large group velocity dispersion (GVD) that can cause serious distortion in a modulated signal in the time domain^[3]. To date, several theoretical and experimental papers have been presented to investigate the dispersion tailoring schemes that aim to realize a wide band and low GVD slow light, with a high group index n_g in photonic crystal waveguides. These methods mainly include reducing the waveguide width^[4,5], chirping the waveguide structure^[6,7], perturbing the radius of air holes^[8,9], introducing ring-shaped holes^[10], simultaneously shifting the first and second rows of air holes^[11–13] adjacent to the waveguide, infiltrating microfluid into the air holes^[14], embedding quantum dots^[15], solely shifting the third row of air holes^[16], and merging coupled cavities^[17]. All these conventional methods tailor the dispersion relation of the guided modes, mainly by modifying the position of the scatter elements, configuring the refractive index profiles by changing geometrical shapes, or infiltrating different materials for the scatter elements in the primitive cell adjacent to the line defect. Another resource that can be utilized to tailor the dispersion relation of guided modes is the angular property of scatter elements. However, no studies have been

conducted to improve the slow light transmission in a photonic crystal waveguide using this valuable property. In this letter, the applicability of a dispersion tailoring approach based on the angular properties of the scatter elements is investigated. In addition, a polyatomic photonic crystal waveguide, including two scatter elements with different geometrical shapes in each primitive cell, has been proposed to realize slow-light transmission to verify the proposed method. Utilizing the angular properties of the scatter elements, the dispersion relation of the guided modes was carefully tailored to achieve slow-light waveguides exhibiting high group index values with small GVD and large bandwidth. Finite difference time domain (FDTD) simulations were also performed to demonstrate the vanishing GVD, enabling the optical signal to propagate with decreasing distortion in the proposed slow-light waveguides.

A diatomic photonic crystal slab with lattice constant a in a dielectric background ($\epsilon = 16.2$) was assumed as the basic structure. This structure can be obtained by the overlay of the square lattice B with circular air holes of radius r on top of the square lattice A with square air holes of width w , as shown in Fig. 1(a). The added lattice B has the same lattice constant a , but is displaced with respect to the lattice A by $a/\sqrt{2}$ along the ΓM direction. Thus, each primitive cell now contains two different scatter elements, i.e., circular and square air holes. The radius of the circular air holes is $0.1a$, and the width of the square air holes is $w = 0.65a$, where a is the lattice constant. In recent years, great improvements have been achieved in the semiconductor processing technology to fabricate various nanostructures. Jones *et al.* showed that a photonic crystal, with a hole diameter of ~ 115 nm, can be manufactured by the step and flash imprint lithography^[18]. Bayat *et al.* fabricated a square-hole photonic-crystal-based polarization converter using standard photolithography and anisotropic deep reactive ion etching processes^[19]. In this letter, the square hole

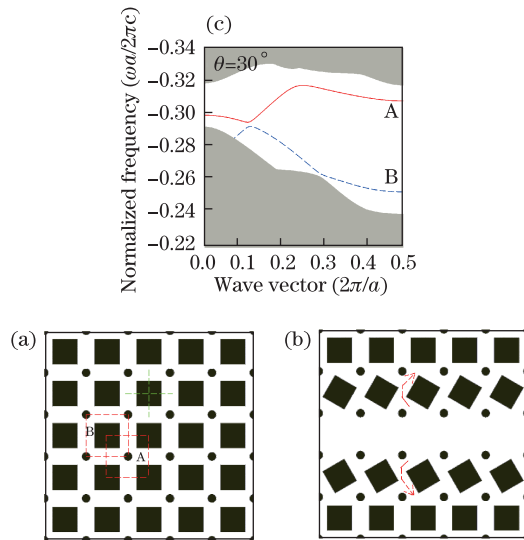


Fig. 1. (Color online) Schematic of the polyatomic photonic crystal geometry (a) intact structure, (b) line defect waveguide, and (c) photonic band of the main propagation mode.

has a width of 322 nm and the diameter of the circular hole is approximately 100 nm when the operating wavelength is 1550 nm. Hence, realizing the proposed structures in practical fabrications is feasible.

A slow light waveguide can be constructed by filling the center square holes with the same background dielectric material of a perfect polyatomic photonic crystal slab. Figure 1(c) shows the dispersion diagram of the photonic crystal waveguide in Fig. 1(b), calculated by the plane wave expansion (PWE) method using MIT's freely available software MPB^[20]. From this plot, the proposed waveguide can provide two propagation modes in the frequency region of interest. Mode A is shown by a red solid line, whereas mode B is represented by a blue dashed-line in Fig. 1(c). Considering that mode B will gradually shift towards the dielectric bands when the subtle structural modification is implemented, only the transverse-electric-like mode A that has a magnetic field parallel to the vertical direction is discussed in this letter. The square air holes at each side of the line defect were rotated around their central axes to tailor the dispersion relation of the guided modes and realize a wide band and low GVD slow light propagation with high group index n_g , as shown in Fig. 1(b). The rotation angle was denoted as θ . The square air holes above the line defect rotate in the clockwise direction, whereas those under the line defect rotate in the counter-clockwise direction to maintain this structure symmetrical with respect to the mode propagation direction. The primitive cells at each side of the line defect have both horizontal and vertical mirror symmetries without rotation operation, and the corresponding symmetry axes are shown by green dashed lines in Fig. 1(a). The mirror symmetry is broken deliberately when rotation operation is introduced in the first rows of the square air holes adjacent to the waveguide, which can change the local symmetry properties of the polyatomic photonic crystal waveguides and precisely manipulate the dispersion relation of the slow light modes.

To achieve this objective, the rotation angle θ of the square air holes on each side of the line defect increases from 0° to 45° , with an incremental step of 5° , as shown in Fig. 2. The impact of rotation angle θ on the dispersion relation of slow light modes and the movement of the flat band with different values of θ is also investigated. The selected band shifts to a higher frequency, whereas the corresponding slope of the dispersion curve decreases gradually, when θ increases from 0° to 45° .

Given that the slab mode band can be shifted by changing θ , the group index and GVD characteristics of proposed slow light waveguides also depend on the rotation operation imposed on the first rows of the square air holes adjacent to the waveguide. The group index n_g can be written as^[21]: $n_g = c/v_g = cdk/d\omega$, where c is the light velocity in vacuum and v_g is the group velocity of the photonic crystal waveguides. The group index n_g versus normalized frequency for the rotation angle θ is demonstrated in Fig. 3. All calculated n_g curves are U-shaped, and the bottom of this U shape is appropriate to obtain a constant group index with small GVD and large bandwidth. It clearly illustrates the variation tendency of group index n_g induced by the rotation operation imposed on the first rows of the square air holes adjacent to the waveguide. The modulus of the group index n_g and the corresponding normalized frequency increases with the rotation angle θ .

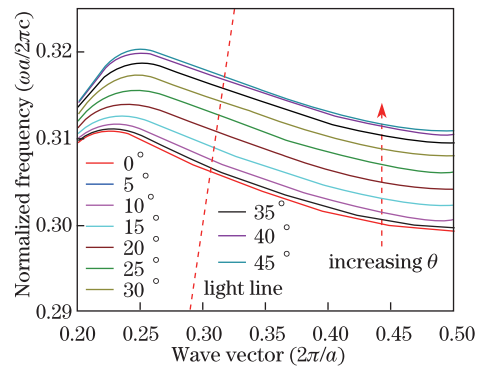


Fig. 2. (Color online) Projected dispersion diagram along the waveguide propagation direction for different θ .

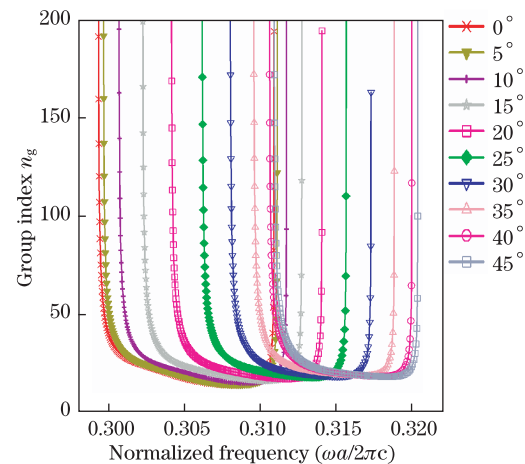


Fig. 3. (Color online) Group index variation versus normalized frequency for different values of θ .

Table 1. Bandwidth, Average Group Index, and NDBP for Our Proposed Waveguides

Rotation Angle θ (deg.)	0	5	10	15	20	25	30	35	40	45
Bandwidth ($\omega a/2\pi c$)	0.0043	0.0043	0.0043	0.0045	0.0046	0.005	0.0052	0.0052	0.0053	0.0055
Average Group Index	14.92	15.17	15.99	17.24	18.21	19.40	19.64	19.63	19.64	19.56
NDBP	0.2085	0.2118	0.2229	0.2506	0.2694	0.3107	0.3253	0.3235	0.3288	0.3394

Linear group velocity dispersion can be characterized by the GVD parameter β_2 and is defined as $\beta_2 = d^2k/d\omega^2$. Figure 4 illustrates the values of the GVD parameter β_2 at different values of the rotation angle θ . For a given θ , the values of β_2 drop from positive GVD (more than 1×10^6 ($a/2\pi c^2$)) to negative GVD (less than -1×10^6 ($a/2\pi c^2$)) by several orders of magnitude with an increase in normalized frequency. Taking $\beta_2 < 10^6$ ($a/2\pi c^2$) as a low GVD, all our proposed waveguides are considered low GVD devices^[22,23]. The minimal GVD exists in the middle region, which then increases the corresponding group velocity in this region. Considering the practical application requirement, feasible slow light regions with a relatively small GVD can be selected.

The average group index and corresponding bandwidth value with different rotation angles θ were calculated. The average group index can be evaluated by Ref. [24] $\tilde{n}_g = \int_{\Delta\omega_0}^{\omega_0+\Delta\omega} n_g(\omega) d\omega / \Delta\omega$, where $\Delta\omega$ represents the slow light bandwidth, defined as the wavelength range corresponding to a maximum of 10% n_g variation with respect to the average group index. The corresponding results under different rotation angles θ are shown in Table 1. The maximum bandwidth and average group index were 0.0055 ($2\pi c/a$) and 19.638, respectively. Based on these results, the normalized delay-bandwidth product (NDBP), defined as the product of the average group index and bandwidth^[25], can be evaluated. The maximum NDBP was 0.3394 when θ is increased from 0° to 45° , which was obtained at 45° for the rotation angle θ and was sufficiently large for the possible use of tunable slow light photonic crystal waveguides in optical buffers. References [10,22], which tailored the dispersion relation of the guided modes based on a unique geometrical parameter, have been selected to compare the results of their devices with our NDBP. The NDBP value calculated in Ref. [22] was 0.3141 for $\tilde{n}_g = 11$, whereas the NDBP in our design was 0.3394, with even a higher group index of 19.65. In Ref. [10], the average group index for the NDBP value of 0.19 is 37, whereas a wider range of NDBP from 0.2085 to 0.3394 and a corresponding average group index of at least 14.92 were achieved in our design.

Pulse light propagation through optimized waveguides was simulated using the FDTD method. The structure with a rotation angle $\theta = 30^\circ$ and a total length $L = 100a$ was chosen to verify the results in the frequency-domain calculation of the photonic bands. Perfectly matched absorbing boundary layers were applied to the structure surroundings in the FDTD simulation. A Gaussian pulse source, centered at a normalized frequency of approximately 0.314965 ($2c/a$) and has a frequency width of $\Delta\omega = 0.0003$ ($2c/a$), was located inside the structure. The optical coupling between a strip waveguide and

our structure is more challenging than the conventional photonic crystal waveguide because of the exotic mode profile in the proposed waveguide. However, several approaches, such as the method presented by Ref. [26], can be used for reference to solve this problem. Considering that the input and output coupling issues are not included in the scope of this study, these issues will be addressed in the future. Figure 5 illustrates the normalized pulse shapes corresponding to the time step propagation through the input and output detecting points in the line defect waveguide. The input detecting point was positioned at $20a$ behind the input port, whereas the output detecting point was positioned at $20a$ before the output port. Hence, the distance L_d between these points was $60a$. The group index can be obtained by dividing the delay time between the two peaks by the transmission length. Figure 5 shows that the total delay time t_d between the two peaks was approximately $989a/c$. Thus, the calculated n_g according to the FDTD simulations was $t_d/L_d = 16.5$, which deviated slightly from the result of $\tilde{n}_g = 19.64$ obtained by the PWE calculation. Considering the different bandwidths selected in the

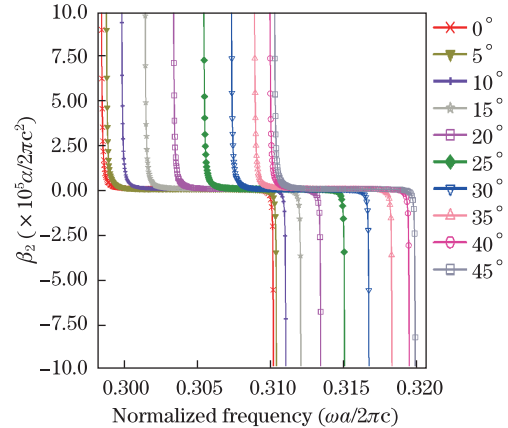


Fig. 4. GVD parameter versus normalized frequency for different values of θ .

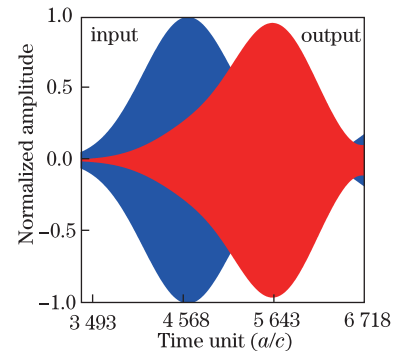


Fig. 5. Temporal pulse propagation at two selected detection points of $20a$ and $80a$, respectively, behind the light source.

two methods, this difference was within a reasonable range. The full-width at half-maximum (FWHM) of the incident and output optical pulses were $1248a/c$ and $1261a/c$. Hence, the pulse width was broadened only by 1.04%, which leads to the conclusion that the signal can be transmitted without obvious distortion because of the low dispersion and limited simulation length of the waveguide. The peak value of the output pulse was slightly reduced compared with that of the input pulse because of the dispersion-induced pulse broadening. In addition to this degradation effect, no obvious reduction in the peak amplitude of the output pulse was observed in Fig. 5. In our simulation works, the light source generated two wave pulses in opposite directions. The forward-propagating pulse transmits along the waveguide axis and corresponds to the first peak of the input pulse. Meanwhile, the backward-propagating pulse arrives at the boundary and is reflected back to the waveguide, resulting in the second peak of the input pulse at an approximate time unit of 6718.

The dispersion tailoring method proposed in this letter, based on the angular properties of the scatter elements, can achieve a wide range of applications in the photonic crystal waveguides, especially for the polyatomic photonic crystals. Compared with the monoatomic photonic crystals, the polyatomic photonic crystals can provide numerous competitive advantages because of the lattice symmetry variation caused by the addition of different scatter elements into each primitive cell^[27]. For example, considering a polyatomic photonic crystal that only contains the circular-shaped scatter element, the multiple different scatter elements existing in each primitive cell can be brought together into a rigid group that can present some angular properties although these circular-shaped scatter elements do not show any angular property. Thus, these groups of scatter elements can be rotated around their central axes to tailor the dispersion relation of the guided modes. Utilizing the local symmetry properties of polyatomic photonic crystals and the method proposed in this letter, additional smart and effective optimization schemes can be established to fabricate slow light devices with enhanced performance properties.

In conclusion, slow-light transmission for photonic crystal waveguides is studied in terms of the angular properties of the scatter elements. The dispersion relation of the guided modes is sensitive to the rotation operation of the scatter elements, and the wide band and low GVD slow light waveguide with high group index can be achieved if this approach is utilized. In addition, the numerical results extracted from the PWE method and FDTD simulations demonstrate the feasibility of our method. The proposed approach can fully explore the impact of local symmetry variation on the dispersion relation of the guided modes. More smart and effective optimization schemes based on this approach can be established to fabricate slow light devices with enhanced performance properties.

This work was supported by the National “973” Program of China (No. 2010CB328204), the National Natural Science Foundation of China (Nos. 60932004 and 61167005), the National “863” Program of China

(No. 2012AA011301), the RFDP Project of China (No. 20090005110013), the “111” Project of China (No. B07005), and the Natural Science Fund of Gansu Province of China (No. 1112RJZA017).

References

1. L. V. Hau, S. E. Harris, Z. Dutton, and C. H. Behroozi, *Nature* **397**, 594 (1999).
2. D. F. Philips, A. Fleischhauer, A. Mair, R. L. Walsworth, and M. D. Lukin, *Phys. Rev. Lett.* **86**, 783 (2001).
3. R. J. P. Engelen, Y. Sugimoto, Y. Watanabe, J. P. Korterik, N. Ikeda, N. F. van Hulst, K. Asakawa, and L. Kuipers, *Opt. Express* **14**, 1658 (2006).
4. Yu. Petrov and M. Eich, *Appl. Phys. Lett.* **85**, 4866 (2004).
5. M. D. Settle, R. J. P. Engelen, M. Salib, A. Michaeli, L. Kuipers, and T. F. Krauss, *Opt. Express* **15**, 219 (2007).
6. D. Mori and T. Baba, *Appl. Phys. Lett.* **85**, 1101 (2004).
7. D. Mori and T. Baba, *Opt. Express* **13**, 9398 (2005).
8. L. H. Frandsen, A. V. Lavrinenko, J. F. Pefersen, and P. I. Borel, *Opt. Express* **14**, 9444 (2006).
9. S. Kubo, D. Mori, and T. Baba, *Opt. Lett.* **32**, 2981 (2007).
10. A. Säynätjoki, M. Mulo, J. Ahopelto, and H. Lipsanen, *Opt. Express* **15**, 8323 (2007).
11. J. T. Li, T. P. White, L. O’Faolain, A. Gomez-Iglesias, and T. F. Krauss, *Opt. Express* **16**, 6227 (2008).
12. F. C. Leng, W. Y. Liang, B. Liu, T. B. Wang, and H. Z. Wang, *Opt. Express* **18**, 5707 (2010).
13. J. Wu, Y. P. Li, C. Peng, and Z. Y. Wang, *Opt. Commun.* **283**, 2815 (2010).
14. M. E. Heidari, C. Grillet, C. Monat, and B. J. Eggleton, *Opt. Express* **17**, 1628 (2009).
15. T. R. Nielsen, J. Mørk, and A. V. Lavrinenko, *Compt. Rendus. Physique* **10**, 957 (2009).
16. Y. Hamachi, S. Kubo, and T. Baba, *Opt. Lett.* **34**, 1072 (2009).
17. K. Üstün and H. Kurt, *Opt. Express* **18**, 21155 (2010).
18. C. Jones, D. Lentz, G. Doyle, M. Miller, M. Ganapathisubramanian, X. M. Lu, D. Resnick, and D. L. LaBrake, *Proc. SPIE* **6486**, 64860Q (2007).
19. K. Bayat, S. K. Chaudhuri, S. Safavi-Naeini, and M. F. Baroughi, *J. Lightwave Technol.* **27**, 5483 (2009).
20. S. G. Johnson and J. D. Joannopoulos, *Opt. Express* **8**, 173 (2001).
21. J. Ma and C. Jiang, *IEEE J. Quantum Electron.* **44**, 763 (2008).
22. R. Hao, E. Cassan, H. Kurt, J. Hou, X. L. Roux, D. Marris-Morini, L. Vivien, D. S. Gao, Z. P. Zhou, and X. L. Zhang, *IEEE Photon. Technol. Lett.* **22**, 844 (2010).
23. R. Hao, E. Cassan, H. Kurt, X. L. Roux, D. Marris-Morini, L. Vivien, H. M. Wu, Z. P. Zhou, and X. L. Zhang, *Opt. Express* **18**, 5942 (2010).
24. R. Hao, E. Cassan, X. L. Roux, D. S. Gao, V. D. Khanh, L. Vivien, D. Marris-Morini, and X. L. Zhang, *Opt. Express* **18**, 16309 (2010).
25. H. Kurt, K. Üstün, and L. Ayas, *Opt. Express* **18**, 26965 (2010).
26. C. Y. Lin, A. X. Wang, W. C. Lai, J. L. Covey, S. Chakravarty, and R. T. Chen, *Opt. Lett.* **37**, 232 (2012).
27. D. B. Wang, J. Zhang, L. H. Yuan, J. L. Lei, S. Chen, J. W. Han, and S. L. Hou, *Opt. Commun.* **284**, 5829 (2011).